

# An Ocean Model's Response to Scatterometer Winds

Robin Tokmakian

Department of Oceanography, Naval Postgraduate School, Monterey, California

## Abstract.

Two simulations of the North Atlantic have been run using the POP ocean model for approximately two and one half years each. One simulation used the  $1.25^\circ$  wind product from ECMWF and the other used the JPL Quikscat  $0.25^\circ$  gridded product. The resulting sea level anomaly fields from the simulations are quantified by using tide gauge and altimetric sea level anomaly data. In addition, upper ocean quantities were compared, such as the mix layer depths, to understand the difference in the ocean's response when using the different wind products. The analysis found that significant improvements were made in the representation at the surface, and in particular areas where comparison data exists such as the Labrador Sea, there was also improvement in the scatterometer forced run in the depth of the mixed layer.

## 1. Introduction

Several sets of gridded scatterometer fields have been made available for use in forcing the surface an ocean model (e.g. JPL, Florida State, Kelly [2001], O'Brien and Bourassa [2003]). The data set has been increasing in accuracy and length of its observation period for several years and is now of reasonable length to assess its use for secondary purposes. Scatterometer data processing gives fields of wind vectors which are representative of the wind field close to the ocean's surface [Lui and Katsaros, 2001]. Such fields, when translated into fields of wind stress can be used to force the momentum equation at the surface of an ocean model.

Limited studies have been done with these newly created maps of scatterometer wind fields to examine their influence on the circulation fields within an ocean model [e.g. Milliff, et al., 1999, Verschell et al. 1999]. Milliff, et al. [1999] describe the oceanic response in a coarse ( $\tilde{4}^\circ$ ) resolution global model when forced with either an NCEP product or an scatterometer product which repeats annually. They attribute much of the differences in the two simulations to the large scale differences in the mean surface wind fields and not to atmospheric mesoscale features. Additionally, Verschell et al. [1999] describe the results of forcing a 1-1/2 layer, reduced gravity, nonlinear, hydrodynamic tropical model forced with various wind products and conclude that the scatterometer winds quantitatively improve the representation of the sea level.

The research discussed here takes the use of scatterometer winds a step further by applying the winds to a high resolution ocean model to evaluate the changes in how an ocean model responds to such forcing. The paper presents the results of analyses performed on the output of two ocean simulations which are forced respectively with a wind field from the output of a meteorological model (ECMWF) and with a field created from the wind vectors that are measured by the NASA Quikscat instrument. First, a description of the  $0.1^\circ$  resolution, primitive equation model is given, followed by a section describing the wind field and how the stress field was created to drive the ocean model. Next, the analyses are described which include comparisons to in situ and satellite measurements. This section is followed by a summary of the results with some final thoughts about the use of the scatterometer fields in studies of the ocean's circulation field at various frequencies and wavelengths.

## 2. Description of the ocean model and forcing fields

The ocean model whose variability is examined in this paper is the Parallel Ocean Program (POP) model. It has a resolution of  $0.1^\circ$  at the equator with 40 levels. It is configured for the North Atlantic basin; the domain is defined as  $20^\circ\text{S} - 72^\circ\text{N}$  and  $98^\circ\text{W} - 17^\circ\text{E}$  which includes the Gulf of Mexico and the western Mediterranean Sea. It uses a Mercator grid resulting in horizontal resolutions varying from 11.1 km at the equator to 3.2km at the northern boundary.

The horizontal spacing of this grid is less than or equal to the first baroclinic Rossby radius which results in eddies being reasonably well resolved up to approximately 50 degrees latitude [ *Smith et al.*, 2000, Fig. 1]. POP has an implicit free surface and includes mixed layer dynamics [ *Dukowicz and Smith*, 1994]. The *Large et al.* [1994] mixed layer formulation, K- Profile Parameterization (KPP), is active in the simulations. The simulations were initialized from previously spun-up simulations. The output of the simulations was saved daily. The analysis uses a time series of 2 years, 2000 and 2001.

Two simulations are used in the analyses that follow. The first simulation was forced with daily varying wind stresses derived from the European Centre for Medium Weather Forecasting (ECMWF run,  $1.25^\circ$  grid) analysis product for the years spanning 1999 through 2001. The second simulation (SCAT run) was forced with a product that used the daily gridded wind vectors provided by the NASA Pathfinder [ *Kelly*, 2001] measured by Quikscat satellite scatterometer instrument ( $0.25^\circ$  grid). Because of the sampling of the earth's surface by the satellite, small holes exist in the gridded product each day. These holes migrate daily around the global grid. Thus, some pre- processing of the wind field is required to produce a complete field to force the ocean model. Various methods were tried to produce a realistic field and in the end, the holes were filled with fields from the ECMWF product from the same time and smoothed to transition from one product to the other. Figure 1 shows an example of the original field (a) and the (b) shows the holes filled with the vectors from the ECMWF product. It is easily seen that the holes of the original product are relatively small ( $< 2^\circ$  wide and  $20^\circ$  long) and at latitudes between about  $10^\circ$  and  $30^\circ$  N. Because the holes migrate from day to day, the mesoscale structure in the wind fields is compromised only slightly. And as later seen in section 5, the oceanic response between the two simulations is similar in this region and so any concern that this blending of products is not a primary concern for this application.

### 3. Analyses

#### 3.1. Mean Gulf Stream Path

The mean path of the Gulf Stream Extension is shown as an example of the mean field of the two simulation runs. Figure 2 shows a random surface temperature field retrieved from NOAA's public web site which is overlaid with two sets of lines. The first, the solid black lines represents the mean path (average from 2000/2001) from the ECMWF run and the second set of dotted lines represents the path from the SCAT run. The path is defined as the zero SSH contour  $\pm 20$  cm. Although quite similar, the SCAT run has a broader

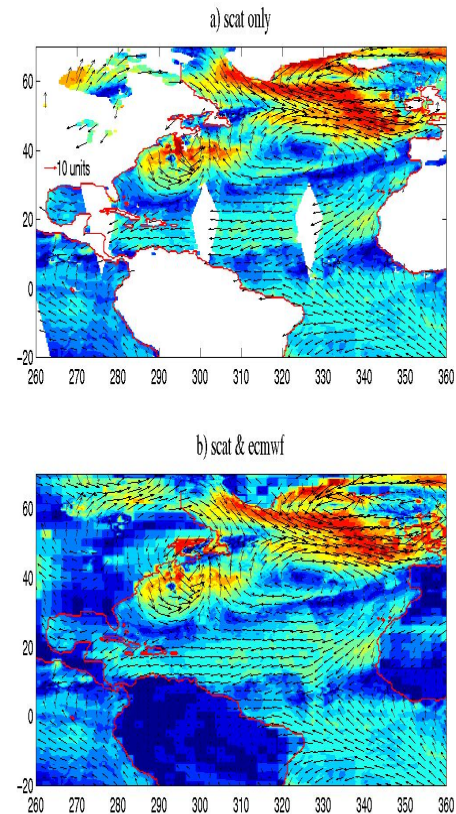


**Figure 1.** a) Daily example of a scatterometer field with amplitude in color overlaid with directional arrows. b) Same figure except with the holes filled in with ECMWF model output. Every tenth vector is plotted.

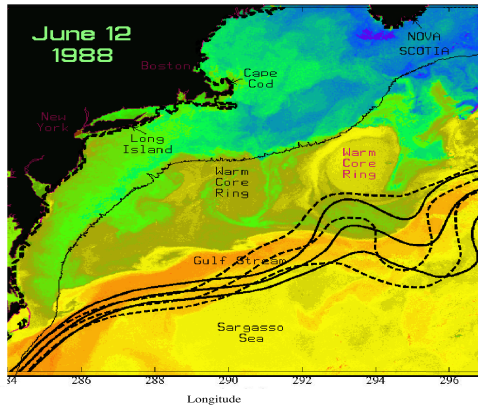


**Figure 2.** Random observed ocean temperature field is overlaid with the contours of the mean path of the Gulf Stream Extension. The solid, heavy black line is the contour for the SSH zero line from the ECWMF simulation, while the dashed line is from the SCAT run.

distribution in its path than does the ECMWF simulation. The bends and turns of the extension diverge towards the eastern edge of the figure. The mean of the two runs are similar throughout the domain with the differences in the small scale (wavelengths  $\lesssim 200$  km) details.

### 3.2. Comparisons to tide gauges

The first, and most robust set used for evaluation is the tide gauge data set from the University of Hawaii [Kilonsky and Caldwell, 1991]. A large number of the time series from coastal stations in this data set were collected over the entire period of the simulation. Daily averages of the sea level data set are used for comparisons to the model's sea level anomaly (SLA) field. The tide gauge daily values are compared directly with the SLA at the time of the model's daily average. Previous papers [e.g. Tokmakian and McClean, 2003] have shown that these types of primitive equation ocean models do well at reproducing the variability of the SLA field with respect to the signal observed by tide gauges. In this paper, we are evaluating whether or not the densely sampled scatterometer fields used to force the ocean improve the SLA signal in the model over the SLA signal that is produced from using a wind field from a meteorological model ( $1.25^\circ$  resolution).

Figure 3 shows the comparison of the correlations be-

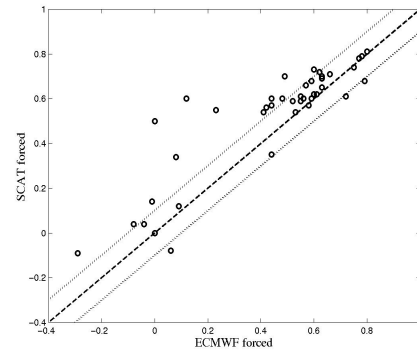


**Figure 3.** Correlations between daily tide gauge measurement and ECMWF SLA simulation (x-axis) and scatterometer SLA simulation (y-axis). Dotted lines denote 10% difference line between the two correlation sets. Dashed line denotes the line corresponding to identical values.

tween the two simulations model SLA and the SLA as measured from the tide gauges. The bottom axis references the correlations when the model is forced with ECMWF winds and along the vertical axis, the correlation values when the model is forced with the scatterometer winds. In all locations, except for four, the correlations have improved for the simulation forced with scatterometer fields. Of the 39 stations compared, 22 have a significant correlation ( $R$  values) of greater than 0.4 and of these, 10 improved their value by 10% when the scatterometer winds were used. For example, the improvement at Sabine Pass, Texas (Figure 4a,  $29.7^\circ\text{N}$ ,  $93.9^\circ\text{W}$ ,  $R=0.7$ : SCAT and  $R=0.6$ : ECMWF) shows that most of the improvement is in the amplitude of the signal, rather than in the phasing. Both simulations miss the large increase in amplitude in the tide gauge signal around March of 2001, perhaps related to a remotely forced event, not represented in the simulation. At Ponta Delgada ( $R=0.6$  and  $R=0.1$ , location =  $37.7^\circ\text{N}$ ,  $25.7^\circ\text{W}$ , Figure 4b), the improvement is in the long period trend of the signal.

In summary, to a large extent, the use of a wind field derived from scatterometer measurements from space increased the correlations of the model's SLA to the tide gauge stations slightly. This is not surprising, since the model when driven with the lower resolution ECMWF winds produces realistic variability and these relatively shallow stations are largely reflecting the ocean response to local, wind forcing.

### 3.3. Basin-wide SLA signals

To ease the analyses and processing of the various fields compared in this section, the model fields originally on a  $0.1^\circ$  grid are averaged onto a grid at  $1^\circ$ . The observational

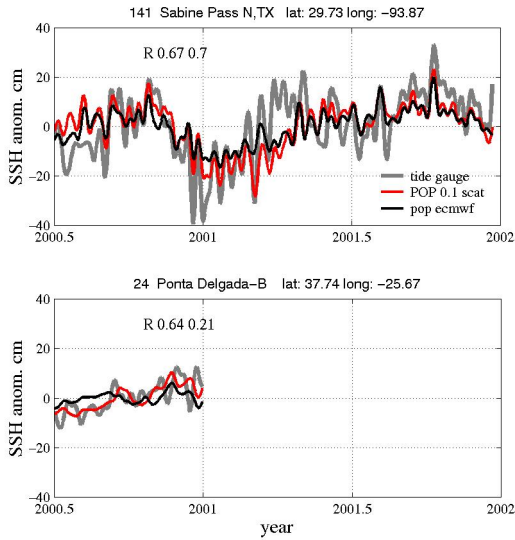


**Figure 4.** Time series of tide gauge SLA in gray, scatterometer run SLA in red and ECMWF run SLA in black for 2 locations a) Sabine Texas and b) Ponta Delgada.

SLA field used for comparison is the French product "Maps of Sea Level Anomalies" (MSLA) produced by the AVISO group at CNES [Ducet, *et. al.*, 2000]. The standard processing has been applied to the altimeter data and the data from a set of satellites have been merged and gridded into 7-day maps at the resolution of  $0.25^\circ$ . The data comes from the TOPEX/Poseidon, GFO, and the multiple ERS satellites. As a further step, to ease the processing and display of the analyses, the data has been further averaged to a grid of  $1^\circ$ .

Figure 5a shows a map of the correlations in SLA between the simulation forced with the ECMWF winds and the one forced with scatterometer winds. At low latitudes, the correlations between the SLA responses of the two ocean simulations are somewhat similar except in an area south of about  $5^\circ\text{S}$ . Likewise, in the coastal regions, which are the shallower regions of the model, the two wind products produce similar results in the ocean's SLA response, consistent with the results of the tide gauge analysis.

Next, the two model simulations are compared with the gridded field produced from satellite measurements of SLA. The analysis has used the fields gridded at  $1^\circ$ , but for graphing purposes, the results show only at every other grid point. The correlations between the SLA of the scatterometer run and the altimeter data are shown in Figure 5b, while the Figure 5c uses the fields of the ECMWF run and the altimeter data. Again similarities in the correlations are extensive between the two simulations. Both simulations show that the

ocean response at latitudes below  $10^\circ$  are reasonable. In addition, the mid-latitude areas which show low correlations in b) and c) are, in the broad sense, areas that show disagreement in the SLA fields of the two model runs. These are areas of mesoscale activity and the disagreement is indicative of the chaotic and unpredictable nature of the flow. More will be said about this in the next section.

To explore where the impact of using the scatterometer winds is significant, the correlations between the modeled fields and the altimeter fields are used along with a measure of skill for each location. Figure 6 attempts to give an indication of the regions where the model has some skill in reproducing the ocean's true response to the wind field applied. The dark gray grid points in Figure 6a are areas where the correlation of the model to the altimeter observations are 0.4 or less and the skill value is less than 10%; meaning that the model is not skillful. The gray areas are regions which have skill in their representation of the true ocean signal and have correlations over 60%. And the rest are areas where the signal can not be distinguished from the noise. The circles on Figure 6 b indicate those areas where the correlations in the SCAT run are greater than the correlations of the ECMWF run by at least 10% as well as having values of 0.4 or greater. In Figure 6 c, the circles denote all the points in the SCAT run with skill and significant correlations over 0.4. The regional area which shows the consistent improvement when the scatterometer winds are used is the area in the eastern tropical Atlantic above the equator centered at  $330^\circ\text{E}$  and along the zonal  $10^\circ\text{N}$  line. The mid-latitudes shows improvement in representation scattered across the mid-latitude grid points, but not consistent improvement over any wide area.

### 3.4. Wave signals

As has been mentioned, the mid-latitudes contain signals that are somewhat chaotic at frequencies of less than a year. Techniques such as radon transforms have been used to examine the wave signal that exists in this frequency band. There have also been many papers written about the Rossby wave signal observed in maps of SLA. The analysis presented in this section uses the radon technique, that many of these papers have used, to explore how Rossby waves observed in the altimeter data fit the theoretical values [Chelton and Schlax, 1997, Killworth, *et al.*, 1997, Cipollini, *et al.*, 1999]. The technique is used here to explore the similarities in the wave energy across a wide range of angles and not only where the maxima of the energy level is located.

Figure 7 shows the estimates of the speeds of westward moving waves at various latitudes for the two runs of the model along with the estimates from the altimetric maps. The fields have not been extensively filtered to iso-

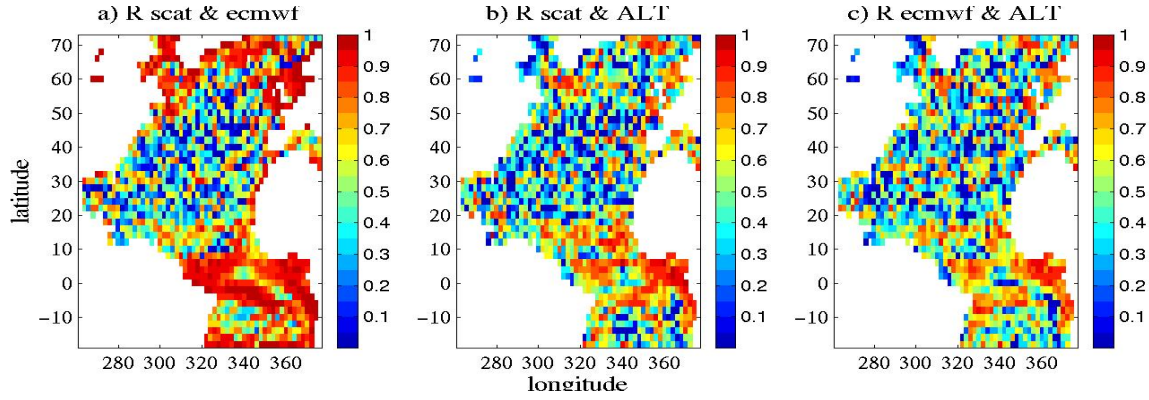


**Figure 5.** Correlations of SLA between a) Scatterometer forced simulation and ECMWF forced simulation, b) Scatterometer simulation and altimeter SLA field, and c) ECMWF simulation and altimeter SLA fields.

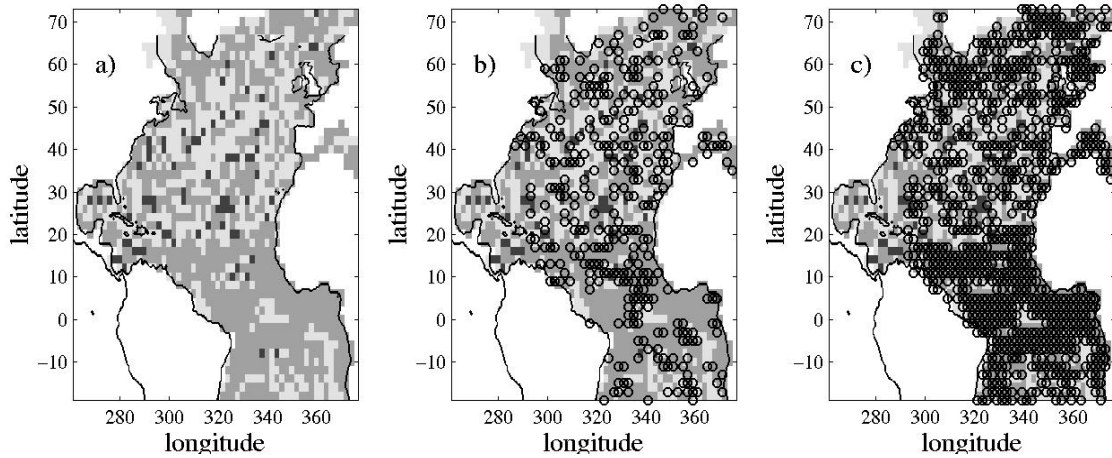


**Figure 6.** a) Map of the model skill to represent the oceanic response of SLA. In both plots, the white areas are low skill areas and the gray areas denote skillful areas. b) same as a) but is overlain with circles which represent grid points where the R value is greater or equal to 0.4 and the SCAT run correlation is 10% greater than the ECMWF run. The right plot (c) is overlain with circles that represent correlations greater than 0.4 for both the ECMWF run and the SCAT run.

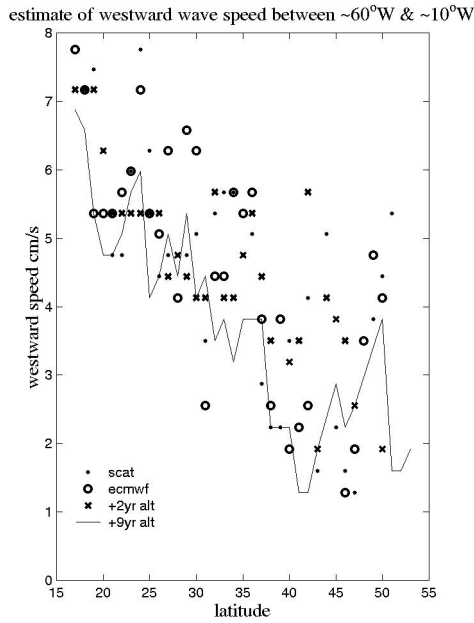


**Figure 7.** Estimates of wave speeds: +9yr altimeter estimate - Solid line, +2 altimeter estimate - x, +2yr ECMWF run open circles, +2yr SCAT run black dots

late, specifically, the westward traveling signals as is done by some researchers [e.g. Cipollini, *et al.*, 1999]. First, it is noted that there is a difference at some latitudes between the +9 year altimetric estimations (solid line) and the +2 year estimates (x's). In addition, the three time series representing a period of +2 year series (black dots - SCAT run, the open circles- ECMWF run, and x's - altimetric data) are also somewhat different. Within the subtropical latitudes ( $15^{\circ}$  -  $35^{\circ}$ ) the two altimetric series are more similar than at the higher latitudes. All the 2+ time series have consistently higher calculated speeds than the 9+ year altimeter series.

A measure of how well the model runs reproduce the estimates calculated from the altimetric observations is given by the ratio of the wave speeds from the model runs to the altimeter data (Figure 8). At the lower latitudes, the ECMWF run shows a closer representation than does the SCAT run, while within the latitude band between  $25^{\circ}$ N and  $35^{\circ}$ N, the SCAT run is more realistic. A measure of variance is represented by the ratio of the +2 year altimetric series to the +9 year series (solid gray line). Fourteen of the twenty SCAT estimates are within this band of variability while only eleven of the twenty ECMWF estimates are within the band. The SCAT ratios not within the band are consistently overestimates of the wave speeds, while the ECMWF run produces ratios that are both over and underestimates.

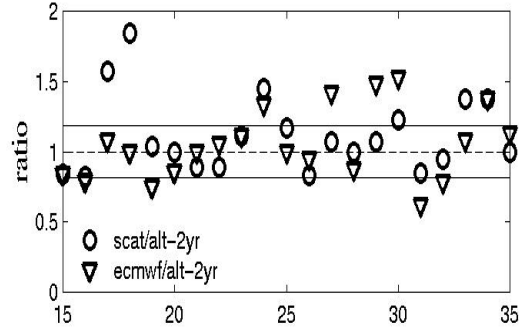


**Figure 8.** Ratio of Rossby speeds, circles: SCAT run/+9yr, triangles: ECMWF run/+9yr. The lines denote the expected variability band determined by the average ratio of the +2yr altimeter signal to the +9yr signal.

The energy as represented by the SLA of the two model runs as a function of angle and latitude are shown in Figure 9a and b, while a similar energy distribution for the +2 year altimeter series is shown in Figure 9c. The most prominent difference in Figure 9a and b is between  $39^{\circ}$ N and  $42^{\circ}$ N, the latitude band of the Gulf Stream (GS) Extension. A qualitative assessment of the difference in the two model runs suggests that the SCAT run (Figure 9b) is the most realistic with a high band of energy distributed across all angles. The other difference is that it would appear that the GS has shifted southward slightly in the SCAT run. It is also noted that in the  $15^{\circ}$ N -  $35^{\circ}$ N band, the energy peak in the SCAT run (b) is spread over a wider range of angles, then in the ECMWF run (a), consistent with the mean path as shown in Figure 2.

In summary, the comparison of the SLA field across the basin shows that the use of the scatterometer derived wind stresses produces a better oceanic response than with the use of the ECMWF wind product. The somewhat chaotic planetary wave response appears to be more realistic when forced with SCAT data than with ECMWF fields.

### 3.5. Mixed layer depth

One of the quantities that is saved during the model runs is the depth of the mixed layer. It is saved on a daily basis. The two simulations, generally, produce similar estimates of the depth of the mixed layer as represented in Figure 10, with the Labrador Sea, the exception. Figure 10a and b represent the mean of the layer's depth for the year 2001 for the SCAT run and ECMWF run, respectively. Figure 10c is the difference of the two means, while Figure 10d represents the standard deviation for the period of a year. The sense of the plot is that the blue regions are regions where the depth of

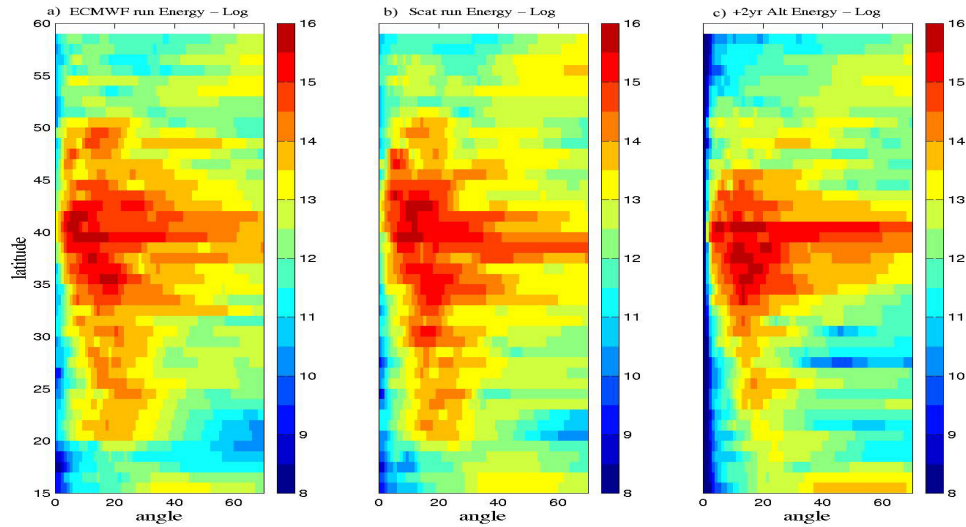


**Figure 9.** Wave energy distribution a) for ECMWF run, b) for SCAT run, c) for +2yr Altimeter data. Scale is a log scale of arbitrary units.

the ECMWF run is deeper than that of the SCAT run and the yellow/red regions are where the SCAT run produces deeper depths or larger variances from the mean. The region of the North Atlantic external to the Labrador Sea shows change similar to the area in the plots around 50-52°N with eddy-like signatures. The difference in both the means and their standard deviations indicate that the most intense difference (greater than 100m) is in a relatively small area centered at 310°E, 58°N. Examining the fields at higher resolution does not seem to indicate that the small scale structure is more defined in the SCAT run verse that seen in the ECMWF run. The general strength of the wind field is similar in both simulations, but there is a higher spatial variability by about 15% in the scatterometer wind field, resulting in a less coherent wind field across the area. This produces a shallower mixed layer in the scatterometer forced run than in the ECMWF forced run.

A time series of the mixed layer depth can be extracted from the output fields and is shown in Figure 11 at a point where the deepest mixing is, 58°N, 51°W. The SCAT run is shown in red and the ECMWF run is the black line for the year 2001. It can be seen that for much of the year the lines are identical. The winter mixing seen during the February/March time frame is distinctly deeper when the model is forced with the ECMWF product than when forced with the scatterometer winds. In situ station data has been collected by IMF Kiel (see: <http://www.ifm.uni-kiel.de/fb/fb1/po1/research/sfb460/a2/sfb-a2.html>) and from that data set, the observed depth more closely represents the

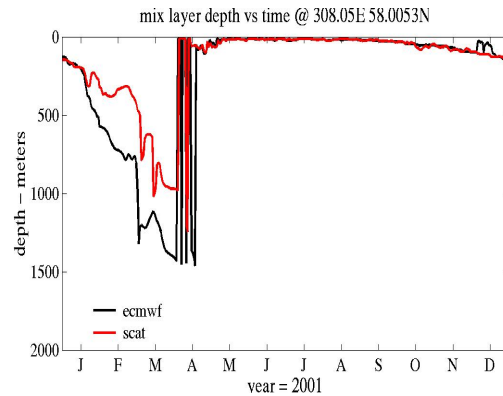


**Figure 11.** Time series of the mix layer depth at a location near Ocean Station Bravo and IMF Kiel stations K1-K41, 58°N, 51°W.

shallower representation of the mixed layer depth of the run forced with the scatterometer winds.

In the subtropics (15°N-30°N), the difference in the mean mixed layer depth between the two simulations is about 2 m with a standard deviation of 10 m for the SCAT run and 9 m for the ECMWF run. If a time-latitude plot is made of the mixed layer depth, along with a plot of SLA at 25°N, interesting differences can be seen. Figure 12 shows how the changes in mixed layer depth change in response to the surface as represented by the SLA. The individual figures have been detrended zonally to remove the large cross-basin

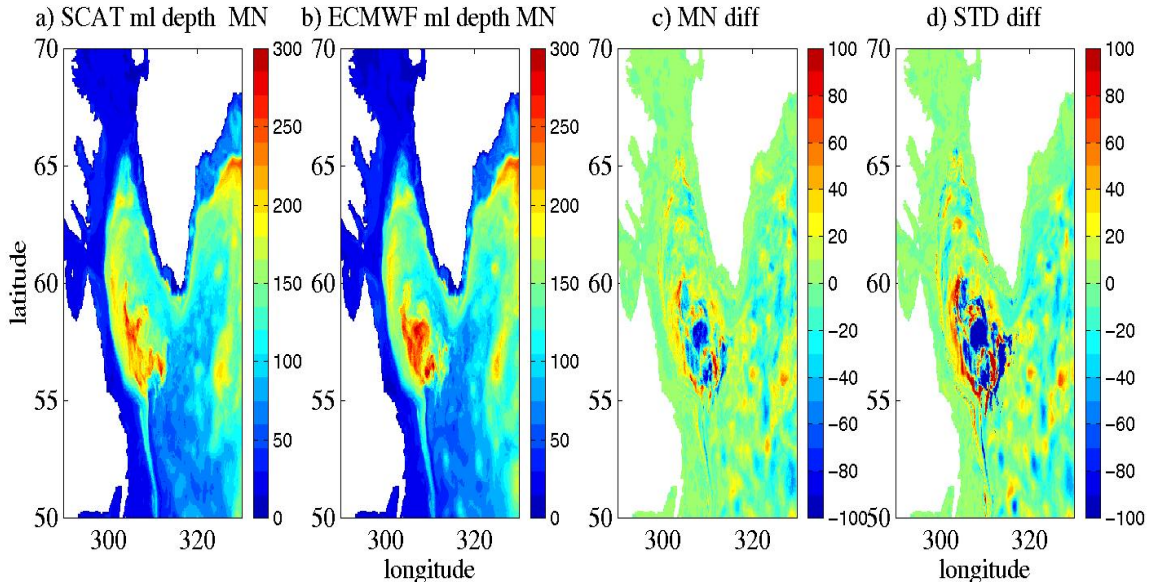


**Figure 10.** a) Mean of Scatterometer run mix layer in Labrador Sea b) same for ECMWF run c) Difference in mean, d) Difference in the standard deviation.

SSH differences and also normalized by the maximum zonal value so as to compare the SLA and the mixed layer depth anomalies (MLA). Clear propagating signals can be seen in both SLA and the MLA. There are differences in the phasing and also in the average speed as was shown in Figure 8. The similarities in the westward wave propagations of the SLA to the mixed layer (a and b, c and d) indicate that the change in the depths and surface heights are related to the N/S advection movement. Within the mixed layer, differences can be seen due to the strength of the mixing during the winter season. For example, during the 2001/2002 winter around 320°E, both mixed layer plots show an additional signal which represents this strong mixing. In areas where both the SLA and the MLA are in phase (290°-310°E, non-winter seasons), and where the SLA is high and the MLA is deep, the signal is clearly produced by a propagating wave moving through a field which has high SLA on the north along with deeper (on average) MLA. During the winter season, the propagation events are out of phase in the SLA and the MLA, with the deeper MLA (more reddish) reflecting a lower SLA. Such representation is more indicative of cooler waters mixing into the upper waters, thus lowering the sea level. Although the mixed layer difference is relatively small as compared to the Labrador sea, the SCAT run shows stronger mixing, spread over a wider band (winter 2000/2001) than is seen in the ECMWF run.

It has been shown how the two simulations differ the variability of the upper levels of the ocean. Clearly there are connections between the processes of the mixed layer and

surface. Whether these differences in the two model runs are important in their connection to ecosystem changes are something that will be investigated at a later date.

#### 4. Conclusions

While previous studies [e.g. Tokmakian 1996] have shown that the seasonal cycle of the SLA is reasonably reproduced in model simulations, the realism of the higher frequency signals are much more difficult to quantify. From these two simulations, it can be argued that there is improvement in the representation of SLA when the scatterometer winds are used, especially in the tropical band. These results are enforce the conclusions of Verschell *et al.* [1999]. One could ask the question of why the correlations are relatively lower (along with a lower skill) in the North Atlantic between 10°N and 50°N? The mesoscale and high frequency signals of the SLA are somewhat chaotic and even with only small differences in the wind fields, significant differences in wave propagation speeds are seen. Whenever possible, scatterometer winds should be used. The only limitation is the length of the time series limits such simulations to a few years if one is interested in long simulations produced with real winds.

**Acknowledgments.** Support for this research has been provided by NASA, under T/P-Jason SWT. The author thanks JPL for providing the gridded wind fields. Thanks also to the French CNES/AVISO group for their gridded and merged fields of altime-

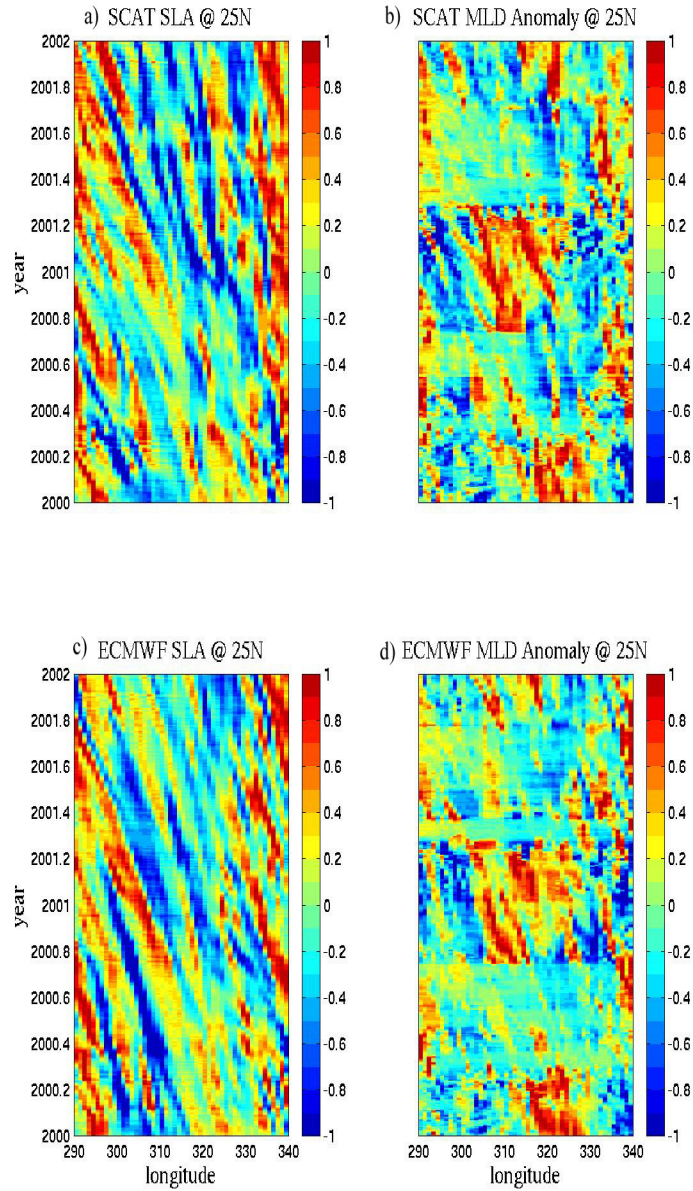


**Figure 12.** Time-latitude plots for a) SLA @25°N SCAT run, b) Mixed layer depth anomal @25°N SCAT, c) SLA @25°N ECMWF run and d) Mixed layer depth anomal @25°N ECMWF. Each series has been detrended across the zone at each time. The field is normalized by the zonal average, and the mixed layer plots (b and d) show in increase in depth as positive (red).

ter SLA and the Univ. of Hawaii Sea Level Center for the tide gauge data. The computing resources were provided for by the Dept. of Defense High Performance Computing Modernization Office, ARL.

## References

- Cipollini, P., D. Cromwell, and G. D. Quartly, Observations of Rossby Wave propagation in the Northeast Atlantic with TOPEX/POSEIDON altimetry, *Adv. Space Res.*, 22, 1553-1556, 1999.
- Ducet, N., P.-Y. Le Traon, and G. Reverdin, Global high resolution mapping of ocean circulation from TOPEX/Poseidon and ERS-1 and -2, *J. Geophys. Res.*, 105, 19477-19498, 2000.
- Dukowicz, J. K., and R. D. Smith, Implicit free-surface method for the Bryan-Cox-Semtner ocean model, *J. Geophys. Res.*, 99, 7991-8014, 1994.
- Ebuchi, N., Graber, H.C., Caruso, M.J. Evaluation of wind vectors observed by QuikSCAT/SeaWinds using ocean buoy data *Jrnl. of Atmospheric and Oceanic Technology*, 19, 2049-2062, 2002.
- Killworth, P. D., D. B. Chelton, and R. de Szoeke, The speed of observed and theoretical long extratropical planetary waves. *J. Phys. Oceanogr.*, 27, 1946-1966, 1997.
- Kilonsky, B. and P. Caldwell, In the pursuit of high quality SL data, *IEEE Oceans Proceedings*, 2, 669-675, 1991.
- Large, W. G., J. C. McWilliams, and S. C. Doney, Oceanic vertical mixing: a review and a model with a nonlocal boundary layer parameterization. *Rev. Geophys.*, 32, 363-403, 1994.
- Liu, W.T., and K.B. Katsaros, Air-Sea Flux from Satellite Data. Ocean Circulation and Climate. G. Siedler, J. Church, and J. Gould (eds), Ch. 3.4, 173-1179, Academic Press, New York, 2001.
- Milliff, R.F., W.G. Large, J. Morzel, G. Danabasoglu and T. Chin, Ocean General circulation model sensitivity to forcing from scatterometer winds. *J. Geophys. Res.*, 11337-11358, 1999.
- O'Brien, J. J. and M. A. Bourassa, The best winds for ocean models?, AMS Annual Conference, Feb. 2003.
- Perry, K. L., SeaWinds on QuikSCAT Level 3, Daily, Gridded Ocean Wind Vectors (JPL SeaWinds Project) Guide Document Version 1.1 D-20335, JPL, Pasadena, CA, 2001.
- Shaw, P.-T., L. J. Peitrafesa, D. N. Flagg, R. W. Houghton, and Kuo-Hsu Su, Low-frequency oscillations on the outer shelf in the southern Mid-Atlantic Bight, *Deep Sea Res.*, 41, 253-271, 1994.
- Smith, R.D., Maltrud, M. E., Bryan, R. O., and M. W. Hecht, Numerical simulation of the North Atlantic ocean at  $1/10^\circ$  *J. Phys. Oceanogr.*, 30, 1532-1561, 2000.
- Stammer D., Wunsch C., and Ponte, R. M., De-aliasing of global high frequency barotropic motions in altimeter observations. *Geophys. Res. Lett.*, 27, 1175-1178, 2000.
- Tokmakian, R. T., Comparisons of time series from two global models with tide gauge data, *Geophys. Res. Lett.*, 23, 3759-3762, 1996.
- Vershell, M. A., M. A. Bourassa, D.E. Weissman, J. J. O'Brien, Ocean model validation of the NASA scatterometer winds, *J. Geophys. Res.*, 104, 11359-11373, 1999.

---

R. Tokmakian, Department of Oceanography, Naval Postgraduate School, Monterey, California, 93943, USA, email: robint@ucar.edu

Received April 2002; revised Sept 2002; accepted , 2002 .

---

This preprint was prepared with AGU's  $\text{\LaTeX}$  macros v5.01, with the extension package 'AGU++' by P. W. Daly, version 1.6b from 1999/08/19.